

1 **JN-01152-2015-R3**

2

3 **Looking for symmetry: fixational eye movements are biased by**
4 **image mirror symmetry**

5

6

7 Andrew Isaac Meso*^{1,2,3}, Anna Montagnini¹, Jason Bell² and Guillaume S. Masson¹

8

9 *corresponding author

10 ¹ Institut de Neurosciences de la Timone

11 UMR 7289 CNRS & Aix-Marseille Université

12 27 Bd Jean Moulin

13 13385 Marseille Cedex 05, France

14

15 ²School of Psychology, University of Western Australia,

16 Crawley, W.A. 6009, Australia

17

18 ³Psychology & Interdisciplinary Neuroscience Research Group,

19 Faculty of Science and Technology, Bournemouth University,

20 Fern Barrow, Poole BH12 5BB, United Kingdom

21

22 Keywords: Mirror Symmetry, Eye Movements, Gaze, Visual Sampling, Saccades

23

24 *Article type:* Research Article (revision, May 2016)

25

26 *No of words*

27 Abstract: 162

28 Introduction: 656

29 Methods + Results: 3155

30 Discussion: 1983

31

32 **Abstract (162)**

33 Humans are highly sensitive to symmetry. During scene exploration, the area of the retina
34 with dense light receptor coverage acquires most information from relevant locations
35 determined by gaze fixation. We characterised patterns of fixational eye movements made by
36 observers staring at synthetic scenes either freely (i.e. free exploration) or during a symmetry
37 orientation discrimination task (i.e. active exploration). Stimuli could be mirror-symmetric or
38 not. Both free and active exploration generated more saccades parallel to the axis of symmetry
39 than along other orientations. Most saccades were small (<2deg) leaving the fovea within a 4-
40 degree radius of fixation. The analysis of saccade dynamics showed that the observed parallel
41 orientation selectivity emerged within 500ms of stimulus onset and persisted throughout the
42 trials under both viewing conditions. Symmetry strongly distorted existing anisotropies in
43 gaze direction in a seemingly automatic process. We argue that this bias serves a functional
44 role in which adjusted scene sampling enhances and maintains sustained sensitivity to local
45 spatial correlations arising from symmetry.

46

47 **New and Noteworthy**

48 This work presents the novel finding that small fixational eye movements made by humans
49 viewing synthetic scenes have their directions strongly distorted in the presence of symmetry.
50 The distortion results in a bias parallel to axes of symmetry measured across various task
51 conditions, and found to be persistent for up to 3 seconds. We argue that this automated
52 process serves a functional role for active vision.

53 **1. Introduction (656)**

54 Symmetry is the presence of spatial redundancies that can be mathematically characterised.
55 Bilateral or mirror symmetry is a ubiquitous, well-recognized feature of the living world but
56 there are other forms including invariance during rotation or translation (e.g. a regularly
57 repeated pattern). Perhaps owing to its ecological relevance, perceptual sensitivity to mirror
58 symmetry has been observed in many different species, for instance insects and birds (Delius
59 and Nowak 1982; Giurfa et al. 1996) as well as humans (for review see (Bertamini and Makin
60 2014; Treder 2010; Wagemans 1995)). Indeed, image symmetry has profound influences on
61 human perception, from low-level visual processes combining separate scene elements into
62 coherent objects (Machilsen et al. 2009) to high-level scene interpretation (Driver et al. 1992).
63 These effects pertain to active vision since large, voluntary saccades during scene exploration
64 are preferentially targeted at image parts containing symmetric shapes (Kootstra et al. 2011;
65 Locher and Nodine 1973).

66 Despite the numerous reports of symmetry-driven effects on perception and eye
67 movements, there remain enormous gaps in the understanding of how we can rapidly extract
68 and use symmetry information. Focusing on mirror symmetry, herein we refer to this simply
69 as symmetry, we aimed at shedding light on some of these by characterising the effects of the
70 axis of symmetry on patterns of fixational eye movements. These eye movements occur when
71 exploration is maintained within a limited region of interest of the visual field and are a
72 combination of small saccades, ocular drifts and tremor (Kowler 2011; Rolfs 2009). The small
73 saccades, often called microsaccades, were considered as a purely stochastic behaviour for
74 decades but have recently received a growing research interest. It is widely agreed that
75 microsaccades have a role in countering the gradual fading of perception which occurs when
76 images remain static on the retina over several seconds (Martinez-Conde et al. 2006; Yarbus
77 1967). Today, there remains some contention about what additional role beyond countering
78 gradual fading fixational eye movements may play in vision. A range of roles and causes for
79 each of the types of small eye movements have been suggested. These include, for instance
80 simply bringing objects of interest into the foveola, a stochastic motor component, an overt
81 attention orienting and more recently a critical role in scene sampling (for reviews see
82 (Engbert 2006; Martinez-Conde et al. 2013; Rucci et al. 2016; Rucci and Victor 2015)).

83 Fixational eye movements determine what information is parsed from complex scenes
84 and as a result, it is now increasingly evident that this links them to several key perceptual and
85 attentional processes (Engbert 2006; Hafed and Clark 2002; Laubrock et al. 2010; Otero-

86 Millan et al. 2008; Poletti et al. 2013). We thus reasoned that investigating whether and how
87 symmetry influences fixational eye movements could reveal a previously unknown heuristic
88 applied by underlying low-level and attention mechanisms to facilitate human sensitivity to
89 spatial structure during active vision.

90 We used simplified stimuli composed of randomly positioned dots which are known to
91 elicit a strong perceived symmetric structure (Barlow and Reeves 1979; Wagemans et al.
92 1991). It is important to note that such a vivid perceived structure in dot stimuli does not arise
93 from explicit shape cues, but instead emerges from a particular widely acknowledged property
94 of symmetry which is that it drives perceptual grouping processes (Apthorp and Bell 2015;
95 Treder 2010; Wagemans 1995). Eye movements were recorded while participants either
96 freely explored the stimulus or actively tried to discriminate the axis of symmetry. The goal
97 was to test alternative hypotheses about how symmetric scenes would be sampled in space
98 over time. We found that most saccades were small so that the fovea remained within the
99 central region of the stimulus for all conditions. Interestingly, we demonstrate for the first
100 time with symmetric stimuli that exploratory saccades show a consistent directional bias
101 along the orientation of the axis of symmetry, not perpendicular to it, independent of whether
102 there was a task. These results suggest a role for fixational eye movements in efficiently
103 sampling symmetric scenes.

104

105 **2. Materials and Methods**

106 *2.1 Observers*

107 Seven human volunteer observers (four males, three females) with normal or corrected to
108 normal vision were recruited from the laboratory for this study, including two authors and five
109 participants naive to the purpose of the study. The experiments were carried out following the
110 approval of the Ethics Committee of the Aix-Marseille Université in accordance with the
111 principles of the Declaration of Helsinki. All participants gave their informed written consent.

112

113 *2.2 Stimuli*

114 Stimuli were made up of a total of 512 randomly placed dots (256 black and 256 white)
115 within a diameter of $D=23.4^\circ$ of visual angle on a grey background area of luminance
116 25.8cd/m^2 . Each square dot had a size of 0.117° and the minimum distance between dots
117 enforced during random placement was $m=0.234^\circ$. The positioning of each dot in polar
118 coordinates $P_i(r_i, \theta_i)$ was implemented using a standard Matlab function (rand) to generate a

119 pair of random numbers from a uniform distribution between zero and one. The resulting
120 components of the polar vector were $\theta_i = 180 \times rand()$ in degrees of orientation angle and
121 $r_i = D \sqrt{rand()}/2$ in degrees of visual angle, where the square root of $rand()$ ensured that density
122 was preserved across the stimulus diameter by correcting for the square in the radius-area
123 relationship. If there was already a dot within the minimal proximity of m , a given placement
124 position P_i was excluded and re-generated until it was valid. Asymmetrical stimuli were
125 generated by applying the dot positioning to the entire stimulus area. Symmetrical stimuli
126 however, were constrained to placement within one half of the circular area and a mirror
127 reflection of the same set of positions were applied onto the blank half (see Figures 1A-C).
128 Stimuli were generated on a Mac computer running OS 10.6.8 and displayed on a Viewsonic
129 p227f CRT monitor with a 20" visible screen of resolution 1024x768 at 100Hz. Task routines
130 were written using Matlab 7.10.0. Video routines from Psychtoolbox 3.0.9 were used to
131 control stimulus display (Brainard 1997; Pelli 1997). Eye movements were recorded using an
132 SR Eyelink 1000 video eye tracker.

133

134 2.3 Procedure

135 Participants sat 57cm in front of a screen with head movements restricted by a chin and head
136 rest. Before each trial, a grey screen was presented for 250ms followed by a 0.234° centrally
137 located, black fixation spot which was on for 750ms. As the fixation spot disappeared, an
138 instance of the random dot stimulus was displayed for 3s, followed by 1.5s of the grey screen
139 before the sequence re-started (Figure 1D). First, for the *free exploration* presentation
140 observers were instructed to view each stimulus keeping their gaze within the large stimulus
141 diameter. Each block contained 160 trials [80 symmetrical + 80 asymmetrical]. Symmetric
142 stimuli had either a vertical [40] or horizontal [40] axis of symmetry and conditions were
143 randomised during presentation. Each block lasted ~18 minutes. After a few trials to allow
144 participants to familiarise themselves with the task, there were 4 blocks collected, giving 160
145 trials per symmetry condition and 320 trials for the control asymmetric condition, per
146 participant. Once the data for the *free exploration* had been completed, a second experiment
147 was carried out. For the *active exploration* presentation, all stimuli were symmetrical and the
148 axis of symmetry (one of four cardinal or oblique axes) had to be discriminated and reported
149 (Figure 1B-D). Stimulus duration, presentation and number of blocks were the same as the
150 free exploration task. Participants were instructed to report the axis' orientation by pressing
151 one of four adjacent buttons corresponding to horizontal (**H**), left oblique (**LO**), vertical (**V**)

152 and right oblique (**RO**). Responses were only recorded during the 3s stimulus presentation
153 time, a longer duration than average response times for the discrimination. Within each block
154 there were 40 randomised presentations of each of the four axes.

155

156 *2.4 Eye movement analysis*

157 Recorded eye movements were cleaned and categorised using standard criteria implemented
158 in bespoke Matlab routines and used for instance to remove blinks and other incidents of lost
159 pupil signal. In order to detect microsaccades, we applied an adaptive velocity-threshold
160 method proposed by Engbert and Kliegl (2003). This method is fully described within the
161 article and here we highlight its key features. A dynamic estimate of speed is calculated from
162 derivatives of a local 5-sample range of raw positions (x - and y - separately). Instantaneous
163 speed estimates are compared against a speed threshold $\lambda\sigma_{x,y}$ with separate x and y
164 components. Speeds above the threshold indicate saccade onsets. In the threshold, $\sigma_{x,y}$ is
165 calculated from a standard deviation based on the local speed median, and not the mean. In
166 the current work we made slight modifications: a value of $\lambda=5$ was used for higher sensitivity
167 instead of a value six used in the original article. We also enforced longer exclusion durations
168 between distinct saccades to avoid artefacts (30ms). Eye position samples composed of
169 saccades, drifts and possible tremors were combined for the six participants (i.e. one
170 participant did not complete the active task) to generate group gaze position density maps.
171 These were analysed by applying the first of two model distribution functions used in the
172 present work, a two-dimensional elliptical Gaussian, to characterise spatial distributions of
173 gaze (see Appendix: section 1). These 2D eye position distributions were generated by
174 assigning valid samples for each of the conditions into a 300 by 300 bin square with sides of
175 24° of visual angle (0.08° bins). For visualisation, these heat maps were re-sampled into 50 by
176 50 bins of 0.48° sides displayed over the stimulus area using an 8-bit pixel colour scale. In
177 each heat map, the pixel of maximum density is identified and its density calculated as a
178 percentage of the total number of samples. This pixel maximum is given in the key of the
179 figures (Figure 2). The fitting procedure generates parameters corresponding to ellipses
180 enclosing about 68% of data points for display.

181 From all detected saccades, we obtained start and end points, amplitudes and
182 directions. Visual inspection of eye movement traces revealed occasional artefacts (<0.5% of
183 saccades) which were then either excluded or corrected for start and end positions. A four
184 peak Lorentzian function was fitted to one-dimensional saccade direction distributions

185 separately for each participant and for each condition (See Appendix: section 2). These
186 distributions were obtained for all saccades under a given condition by extracting each
187 direction and binning it into one of 50 bins spanning the 360° space, resulting in a width of
188 7.2°. The fitting procedure was used to obtain estimates of the underlying continuous density
189 functions across directions. A statistical comparison can be carried out between the fitted
190 density traces. The mean and variance of the participant-specific best-fitting traces allow a
191 two-sample t-test to be carried out across the bins spanning the full direction space at a
192 significance level of $P < 0.05$. For the free exploration condition we compared fits of direction
193 densities obtained under the control asymmetric condition to those under each cardinal axes-
194 symmetric conditions H and V. For the active exploration condition, a comparison was carried
195 out between pairs of orthogonal direction traces e.g. H-V and LO-RO. From these t-tests, the
196 specific points of significant differences between the traces along the 50 direction bins,
197 particularly around cardinal and oblique axes (see Figures 3D and 5D), indicate whether
198 peaks are (a) perpendicular, (b) parallel or (c) independent of symmetry axes.

199 A Direction-Selectivity Index (DSI) was calculated as the ratio of the number of
200 saccades $N_{\Delta\theta_s}$ within a 40° wedge around a given axis of symmetry in both directions (20°
201 counter clockwise and 20° clockwise) to the total number of saccades. The control condition
202 takes an equivalent wedge from a stimulus presentation in the absence of an axis of
203 symmetry. DSI ($N_{\Delta\theta_s}/N_{tot}$) for each 250ms interval gives a value between 0 and 1, to be
204 compared to the expected value of 0.111 when there is no bias (i.e. 40°/360°) for saccade
205 direction. DSI gives a dynamic indication of the relative extent to which saccades occur along
206 a given orientation by contrasting symmetrical and control conditions.

207

208

[Figure 1]

209

210 3. Results

211 3.1 Gaze position

212 We characterised gaze during the tasks by analysing the 2D shapes of eye position
213 distributions. Valid eye position samples for all participants were used to generate heat maps
214 (see methods). For the control asymmetric stimulus condition, eye positions were largely
215 isotropic (see distribution of orange-red areas in Figure 2A) extending a little along both
216 cardinal axes. When an axis of symmetry was present in the free exploration condition,
217 sampling was extended along this axis either horizontally (Figure 2B) or vertically (Figure

218 2C). Differences between the control and symmetry conditions were quantified by fitting an
219 Elliptical Gaussian function to heat maps (see methods). Ellipses are shown for the each of
220 the three free exploration conditions (continuous line plots) characterised by their x and y
221 centre positions, semi-major and minor axes lengths and ellipse orientation angle θ
222 (Figure 2D). The fits were significant when tested using the non-parametric Kolmogorov-
223 Smirnov test (at a level of $P > 0.05$, see Appendix: sections 1 & 3). The control condition was
224 best fitted by an almost circular ellipse (dark blue continuous line in Figure 2D), a little
225 broader along the V than the H direction. In the presence of a symmetric pattern, ellipses were
226 clearly elongated along this axis (continuous green and purple curves, Figure 2D). Therefore
227 most samples lie close to central fixation, even taking into account elongation along cardinal
228 axes. The area enclosed by these ellipses encompassing 68% of the collected samples is
229 approximately $\sim 20\text{-}30\text{deg}^2$ of visual angle across conditions (see Appendix: section 1). This
230 covers only the central 7% of the stimulus area of 452deg^2 in total. Figure 2E-H illustrates
231 corresponding results for the active exploration conditions, with 4 different orientations of the
232 symmetry axes. The gaze patterns were very similar, with the comparable elliptical fits for the
233 cardinal axes in dashed lines in Figure 2D. The scene sampling is seen to similarly occur
234 along the axes of symmetry, but show a non-significant trend extending marginally further
235 along this axis for active when compared to free exploration, based on the fitted width
236 parameters in the direction parallel to the axis (see Figure 2D, continuous vs dashed traces and
237 Appendix Table 1).

238

239

[Figure 2]

240

241 3.2 Saccade characteristics for free exploration: amplitudes, rates and directions

242 Considering saccades as fast movements which place the fovea within regions of interest, we
243 identified them using standard criteria (Engbert and Kliegl 2003) and computed histograms of
244 various saccade properties. Distributions of saccade amplitudes (sizes) are first computed,
245 assigning values for each recorded saccade into one of 50 bins spanning $0\text{-}12^\circ$ of visual angle
246 (i.e. bin size: 0.24°). These distributions shown in Figure 3A are not measurably modulated
247 by the presence of symmetry (compare the blue trace to the others). Across conditions a
248 similar number of saccades were measured with an average and standard deviation of $5384 \pm$
249 197 per condition. Most were small (small $< 2^\circ$: 3805 ± 117 [71%] and micro $< 1^\circ$: 2688 ± 133
250 [50%]). Saccade rates were then computed by assigning each saccade to one of 50 time bins

251 of 16.67ms width based on onset time over the course of the 3s trial. Rates were found to
252 largely overlap for the control, H and V symmetry conditions, shown in Figure 3B (Control
253 blue trace overlaps with the others). The traces show a peak of approximately 2.5-3 saccades
254 per second at 500ms from stimulus onset and then a gentle decline down to 1.5-2 saccades per
255 second.

256 [Figure 3]

257

258 Saccades generated by the oculomotor system during the different conditions were
259 therefore unchanged in numbers, rates and sizes, but only in the directions as suggested by
260 Figure 2. The distributions of saccade direction in Figure 3C show prominent peaks in the
261 direction parallel to the axis of symmetry where it was present (purple and green traces) and
262 smaller peaks around both these axes in the control (dark blue trace). For data obtained from
263 each participant, we fitted the corresponding histograms with a four-peak Lorentzian function
264 (see methods) and found that the function modelled the empirical distributions when a
265 Kolmogorov-Smirnov test was applied (Appendix: section 3). The average and the standard
266 error of the fitted distribution functions for the seven participants are shown in Figure 3D. We
267 apply a two sample t-test comparing points along each of the pair of cardinal traces (purple
268 and green) to the control condition (blue trace). At critical points of comparison
269 corresponding to the cardinal axes ($0^\circ, 90^\circ, 180^\circ$ and 270°), we find a significant difference
270 between the control and the cardinal direction conditions. For example, at 0° for the H-
271 Control comparison and 90° for the V-Control comparison the directions are both
272 significantly different from the control ($t(12) = 2.23$, $p = 0.046$ for H, and $t(12) = 3.21$, $p =$
273 0.0075 for V). The individual participant data behind this group fitting is shown in Figure 4.
274 The total number of saccades identified per participant is also shown inset for each plot. It can
275 be seen that the peaks lie in the cardinal direction (green and purple lines) which is consistent
276 with the result of the averages of Figures 3C-D irrespective of whether participants are naive
277 or not (two authors are indicated by * after participant ID). The exceptions occur where a low
278 number of saccades (<2500) were recorded during the task, in which case peaks are less
279 prominent. This supports the conclusion that saccades preferentially occur along orientations
280 parallel to symmetry axes (*i.e.* significantly more saccades in the direction parallel to the axis
281 of symmetry).

282 [Figure 4]

283

284 3.3 Active scene sampling: saccades

285 We similarly consider the sampling of the scene by characterising the eye movements
286 recorded during the active task. Participants discriminated the axis of symmetry by pressing
287 one of four buttons corresponding to H, LO, V and RO axes of orientation (see Figure 1).
288 Saccade amplitudes have a similar distribution to those measured under the free exploration
289 conditions when compared across the four symmetry axes conditions in the discrimination
290 task (Figure 5A). The number and proportion of microsaccades ($<1\text{deg}$) were comparable for
291 the active exploration task (i.e. 2647 ± 171 compared to 2687 ± 133 for the free exploration,
292 both 50% of the total saccades). Most saccades ($70 \pm 4\%$) were smaller than 2° .

293 Saccade rates were calculated as done for the free exploration task. Results show
294 largely overlapping curves with an initial suppression before 250ms rising to a peak at 500ms
295 of 2-2.5 saccades per second before a gentle decline from around 1000ms, in Figure 5B. This
296 saccade rate trend is similar to that seen for the free exploration, with the exception that the
297 maximum rate is higher by about 0.5 saccade/second for the active task (compare Figures 3B
298 and 5B). We note that the mean reaction time across participants and conditions is 1.18s, and
299 mean reaction times for the four different axis conditions are indicated by the dotted vertical
300 lines within the figure and plotted in Figure 5C. The most prominent difference in the peak
301 rate between the tasks occurs within a critical decision making epoch for the active task based
302 on reaction time.

303

304

[Figure 5]

305

306 The direction distributions across these four conditions were analysed in the same way
307 as those for the free exploration condition. Peaks were seen to occur in the directions parallel
308 to the axis of symmetry (Figure 5D). Using the fitting procedure applying the summation of
309 four-Lorentzian functions separately for each participant, there was a significant fit for all
310 conditions based on a Kolmogorov-Smirnov test (see Appendix: sections 2-3). When the
311 resulting traces of orthogonal axis conditions are compared in a two sample t-test at the angles
312 corresponding to cardinal and oblique axes (i.e. LO-RO at 45° , $t(10) = 3.28$, $p = 0.008$ and H-
313 V at 90° , $t(10) = 2.26$, $p = 0.047$) the best fitting peaks significantly occur around the
314 respective axes of symmetry shown in Figure 5E, where the standard errors are shown by the
315 light shaded areas. These group results are consistent with the effect seen in the different
316 coloured traces (compare blue to orange and green to purple) for all participants in Figure 6.

317 The average number of saccades for each of the oriented axis conditions combining all
318 participant data is very similar to those recorded for the free exploration task (i.e. 5375 ± 301
319 for active compared with 5385 ± 197 for the passive task).

320 The proportion of correct responses and reaction times give an indication of the
321 relative difficulty of the discrimination conditions. The group data indicates that the tasks
322 were easy and participant responses were over 90% correct (see Figure 5C for reaction time
323 and response performance results). Ranking discrimination performance across symmetry axis
324 orientation conditions according to average percentage correct gives H, V, LO and then RO, a
325 rank order which is the same as the relative strength of the different peaks in saccade
326 directions (see different colours in Figure 5D-E).

327

328 [**Figure 6**]

329

330 *3.4 Dynamics of direction selectivity*

331 In order to investigate the temporal dynamics of the observed modulation of saccade direction
332 by symmetry, we computed a Direction Selectivity Index (DSI) for each 250ms temporal bin
333 from the onset of the visual pattern until the end of the trial. The DSI was defined as the ratio
334 of saccades made within a 40° direction wedge around the axis of symmetry to the total
335 number of saccades (see methods). As a control condition, for each main axis (H, V, RO and
336 LO), we evaluated the DSI by taking into account the saccades executed in the free
337 exploration task during the observation of the asymmetric controls. Figure 7 shows the time-
338 course of the DSI along the horizontal and vertical axes (upper panels), for the active and free
339 exploration tasks, as compared to the control condition. In the lower panels, the DSI estimated
340 in the active task is compared to the control condition for the oblique axes. The vertical dotted
341 lines indicate the mean reaction time for the on-going perceptual discrimination task and the
342 grey shading shows \pm one standard deviation of the recorded values.

343 For all symmetry axes, direction selectivity increases rapidly (within the first 500ms)
344 in the symmetric test conditions and then remains rather constant until the end of the trial,
345 with the exception of the horizontal axis condition where selectivity rises continuously. The
346 control DSI remains nearly constant at a lower level (close to the value expected for a uniform
347 random distribution of saccades, ~ 0.111) for the V, RO and LO conditions. For the horizontal
348 selectivity, the rise of the control DSI in time reflects a bias in favour of the horizontal
349 direction. The red and blue asterisks in Figure 7 indicate the time-bins in which the DSI

350 estimated during the active (red asterisks) and passive (blue asterisks) tasks becomes
351 significantly higher than the control according to the non-parametric Kruskal-Wallis test for
352 mean differences performed at a significance threshold of $P=0.05$ across the range of values
353 within the trace. Notice that the DSIs remained largely stable after the subjects had reported
354 their perceptual decisions showing that the bias persisted over the trial duration.

355 [Figure 7]
356

357 **Discussion (1983)**

358 Symmetry is a ubiquitous feature of objects within our visual environments to which humans
359 and other animals are highly sensitive (Treder 2010; Wagemans 1995). Humans are very fast
360 and efficient at detecting mirror symmetric stimuli (Carmody et al. 1977; Wagemans et al.
361 1991). The perceptual interpretation of complex scenes is also fundamentally affected by
362 symmetry. Ambiguous structure-from-motion stimuli, for example, tend to be perceived as
363 transparent instead of cylindrical in the presence of symmetry (Treder and Meulenbroek 2010;
364 Wallach and O'Connell 1953). At higher cognitive levels, symmetry causes an
365 underestimation of element numbers when compared to estimates from asymmetric controls,
366 possibly due to symmetry-evoked redundancy reduction computations (Apthorp and Bell
367 2015) and human faces are typically judged to be healthier and more attractive when
368 symmetrical (Rhodes 2006). This series of evidence suggests that symmetry has far reaching
369 effects on the fast integrative visual processes combining disparate bits of information to
370 extract the perceptual organisation of complex visual scenes. It is therefore not surprising that
371 symmetry can also influence active vision by determining gaze patterns during visual search
372 tasks (Kootstra et al. 2011; Locher and Nodine 1973).

373 However, the nature of such high sensitivity is still highly disputed between the
374 proponents of symmetry processing being a low level mechanism and those viewing it as a
375 predominantly high-level mechanism. Our strategy was to investigate how fixational eye
376 movements are patterned by axes of mirror symmetry and how such spatio-temporal
377 characteristics of eye movements would depend on the cognitive task at hand. As expected,
378 most eye movements and fixations remained relatively near the stimulus centre. Saccades
379 were generally small (50% or more of saccades were smaller than 1°) and presumably largely
380 involuntary. Thus fixation tended to remain around the 'centre of mass' of the visual stimuli
381 (Findlay 1982; He and Kowler 1989). However, we observed small but highly consistent
382 elongations of gaze distributions along the axes of symmetry. Directions of saccades of all

383 sizes were strongly biased parallel to the axis of symmetry. Previous work looking at saccade
384 direction distributions during an orientation discrimination of textured ellipses showed similar
385 elongations of distributions, which in that case occurred along the longer axis of elliptically
386 shaped stimuli (Hicheur et al. 2013). This was also consistent with other previous findings
387 linking the direction of fixational eye movements to visual task performance. Suppressing
388 certain eye movements directions hindered orientation discrimination (Rucci et al. 2007).
389 Furthermore, in the face of high precision perceptual tasks, goal-directed microsaccades
390 served to finely relocate the visual target to improve performance (Poletti et al. 2013). It has
391 generally been suggested that such fixational eye movements have an additional active
392 sampling role beyond countering visual fading (McCamy et al. 2014; Otero-Millan et al.
393 2008). The currently observed oriented behaviour should therefore result in optimal sampling
394 along the axis in the presence of symmetry. Interestingly, such fixational patterns were
395 identical when observers were instructed to freely view the stimuli or to discriminate the
396 symmetry axis orientation, a challenging perceptual task under some axis orientation
397 conditions. The consistency of this result across tasks suggests that symmetry processing is an
398 automatic mechanism which is at least in part operating at a low level, and as such optimally
399 shapes the constraints on fixation.

400

401 *Evidence for automatic symmetry processing through a sustained saccade direction distortion*

402 The main novelty of the present study is the strong spatial patterning of fixational eye
403 movements in the presence of mirror symmetry. The symmetry axis orientation shaped all
404 types of eye movements. Gaze locations were aligned along it and directions of the
405 predominantly small saccades as well as larger ones were also strongly oriented parallel to it,
406 both demonstrating that fixation maintains the fovea on the symmetry axis and movements
407 explore it over several degrees of visual angle. Our Direction Selectivity Index illustrated the
408 dynamics of the saccade directional bias. We found that the saccadic selectivity for the axis of
409 symmetry started as early as 500ms after stimulus onset and was then sustained until the end
410 of the trial, continuing after the discrimination decision had been made and reported. Such a
411 pattern of temporal dynamics is consistent with human electroencephalography studies
412 showing that event related potentials associated with symmetric presentations are sustained,
413 starting at 250-300ms after presentation onset (Makin et al. 2013; Norcia et al. 2002; Wright
414 et al. 2015). Although it should be noted that most electroencephalography studies monitor
415 and discard trials in which eye movements are produced.

416 The spatio-temporal patterns of fixation along the symmetry axis were the same when
417 subjects were asked to fixate the image (i.e. free exploration) or to perform an orientation
418 discrimination task about the axis of symmetry (i.e. active exploration). In each task, the total
419 number of saccades and the total area covered by fixational movements were only marginally
420 affected by the presence and the orientation of a symmetry axis. The orientation of fixation
421 patterns was however consistently very strongly affected. The exact trajectory of fixational
422 eye movements are often described as a Brownian motion in which the diffusion process can
423 be biased by low level visual features (Engbert 2006; Rucci and Victor 2015). We clearly
424 demonstrate herein that the axis of symmetry is one of these features, acting as an attractor
425 line along which the active eye could optimally structure visual information extraction. The
426 magnitude of this active scanning seems to be scaled (but not qualitatively modified)
427 depending upon the task demand, as suggested by the increasing spread of fixation area along
428 the axis, and the slight increase in saccade rate during the early phase of symmetry
429 discrimination. However, the main spatio-temporal properties of the fixation pattern must be
430 determined by an automatic mechanism detecting the location and orientation of the axis of
431 symmetry as a salient feature of the image and sending this information downstream to the
432 oculomotor system finely controlling fixational eye movements (Hafed et al. 2009).

433

434 *Automatic but not a bug: a role for symmetry axis scanning*

435 The fact that the spatial properties of the symmetry-dependent pattern of fixation remain
436 unchanged when human observers must discriminate mirror symmetry axis orientation argues
437 for an automatic processing of symmetry information and its role in the oculomotor control of
438 the active eye. This should however not be mistaken for evidence against a functional role for
439 fixational eye movements or its adaptability to task-specific constraints. During symmetric
440 orientation discrimination, sampling of the stimulus area extended slightly more along the
441 axis of symmetry. This suggests that the specific fixation behaviour observed with mirrored
442 patterns can be boosted, when required, to adjust coverage area along the symmetry axis. This
443 role could be achieved with a functional contribution by fixational eye movements in the
444 analysis of image symmetry, similar to what has been found for other low-level detection and
445 discrimination tasks e.g. (Martinez-Conde et al. 2006; Poletti et al. 2013; Spotorno et al. 2015;
446 Yuval-Greenberg et al. 2014). In an orientation discrimination task in which a textured
447 elliptical shape was embedded in a luminance noise background, saccade rates were lower for
448 dynamic noise than under static noise within a critical window of about 2s from stimulus

449 onset and directional biases along the longer axis were measured during the same time
450 window (Hicheur et al. 2013). Reaction times were slightly longer on average for dynamic
451 backgrounds, implying the discrimination was more difficult under the condition which also
452 generated fewer saccades and a more stochastic spatio-temporal oculomotor pattern. The
453 explanation for the directional effects of saccades observed were argued in terms of allocation
454 of spatial attention and in that context we note that saccade rates were only comparable to
455 those recorded in the current tasks ($>1.0s^{-1}$) up to about 500ms from stimulus onset.
456 Stimulation with a large simple symmetric stimulus may provide a stronger input than
457 oriented shapes and explain some of the differences. To verify this, the relationship between
458 eye movement patterns and different visual properties that determine image spatial structure
459 (e.g. luminance, shape, symmetry...) needs to be further studied in order to better understand
460 how these different features are weighted and integrated to control fixation.

461 Is the sustained perturbation of saccade generation currently reported over a 3s
462 duration also attributable to allocation of spatial attention along the symmetry axis or does an
463 alternative low-level mechanism provide a more plausible explanation? For symmetry, we
464 lean towards an interpretation of lower level mechanisms both because of the persistence of
465 the effect well beyond the discrimination response and its consistency across active and
466 passive exploration conditions. Coherently, some neurophysiological studies have argued that
467 a direct enhancement of early visual signals (e.g. primary visual cortex) could be achieved by
468 microsaccades. Such selective enhancement however requires that extra-retinal information
469 about eye movements were taken into account by the visual system (Martinez-Conde et al.
470 2013; Troncoso et al. 2015). More empirical evidence is still needed to disentangle the
471 contributions of lower level and cognitive mechanisms to the automatic symmetry processing
472 and in particular to characterise how this relates to spatial attention. Again, a direct
473 comparison between the different visual features related to spatial structure would help in
474 better understanding whether, and how symmetry can specifically shape the interplay between
475 attention and fixation.

476 Two decades of intensive research on visual fixation have overturned the classic view
477 of fixational eye movements. Nowadays, fixational movements are seen as a part of a strategy
478 for an optimal spatio-temporal structuring of the visual inflow (see (McCamy et al. 2014;
479 Rucci et al. 2016; Rucci and Victor 2015)). How can they specifically help in the processing
480 of symmetrical images? Our results clearly rule out two alternative strategies that could be
481 proposed for extracting symmetry information and provide strong evidence for a third

482 plausible alternative. We show that saccades do not predominantly occur in a direction
483 perpendicular to the axis of symmetry, as might be expected if performing point-by-point
484 temporal correlation within the foveal area. Moreover, our results demonstrate that even once
485 symmetry had been detected redundancy was not exploited in the simplest way by exploring
486 only one half of the given dot stimuli. Rather, gaze remained predominantly within the centre
487 of mass of the large stimulus area so that the fovea was continuously drifted over a limited
488 central region of interest. We reasoned that, once integrated over time, such sampling
489 movements parallel to the axis of symmetry would yield a stronger signal for local filter
490 correlations detecting symmetry. A similar scheme was proposed in the retinal models of
491 fixational eye movements which generate sampling improvements by noise enhancement and
492 temporal integration (Zozor et al. 2009). If the role of small saccades is to extend the
493 representation of the dot elements over space and time along the orientation of the axis of
494 symmetry, then after few eye movements aligned with the axis of symmetry, the ‘elongated’
495 dots created by persistent sets of effective dipoles generated at each small saccade become
496 easier to detect with local orientated filters.

497 Finally, our result highlights the need for an extension of standard methods of
498 computing visual saliency based on luminance, colour and orientation filters (Itti and Koch
499 2001; Itti et al. 1998). It has previously been found that symmetry influenced where observers
500 looked in scenes in ways that could not be entirely accounted for by the standard saliency
501 models (Kootstra et al. 2011; Locher and Nodine 1973). Our finding of a profound change of
502 eye movements in the presence of symmetry supports the previous work in proposing that
503 saliency estimation should take local symmetry information into account. This approach was
504 indeed taken by some of the most sensitive computer-vision models (Jenkinson and Brady
505 2002; Marola 1989). In a biologically plausible framework, high sensitivity is achieved by
506 using multi-scale filters similar to those applied to the standard saliency models (Itti et al.
507 1998). Locally pairing luminance filters (i.e. with odd-sine and even-cosine phases) can
508 generate sensitivity to local symmetry (Kovesi 1997; Osorio 1996). Further work extending
509 this framework could prove invaluable in establishing a biologically plausible, canonical
510 computation of hierarchical processing.

511

512 **Acknowledgements**

513 *We thank volunteer participants for their time and the members of the InViBe Team for their*
514 *fruitful discussions. We also thank reviewers for their constructive criticism and suggestions*

Short title: Symmetry axes bias saccade direction

515 *during the peer review process. This research was funded by the Agence National de la*
516 *Recherche (Grant SPEED, ANR-13-SHS2-0006) and the Centre National de la Recherche*
517 *Scientifique (CNRS). JB was supported by Australian Research Council (ARC) grants*
518 *#DP110101511 and #LP130100181. AM was also supported by the Agence National de la*
519 *Recherche (Grant REM, ANR-13-APPR-0008-02)*

520

521

522 **Figure legends**

523 **Figure 1:** Visual stimulus and task. **A.** Control stimulus, made up of black and white dots
524 randomly placed on a grey background within a circular region of diameter 23.4° of visual
525 angle. Dot positioning results in no overall structure. **B.** Mirror-symmetric stimulus,
526 symmetric about the horizontal axis. Light dashed outer circular and straight lines (not shown
527 during experiments) illustrate the stimulus circumference and midline. The smaller circle
528 indicates an 8° diameter within which most gaze samples remained (92-99%). **C.** Left oblique
529 axis of symmetry. Symmetry along this axis is less vivid than on the cardinal axes. **D.** Task
530 illustration: 0.75ms initial fixation followed by a 3s stimulus presentation with eye
531 movements recorded, followed by a 1.5s blank before the sequence re-starts. In the active
532 task, during the 3s presentation the response is recorded through one of four button presses
533 corresponding to the axes.

534

535 **Figure 2:** Gaze positions from eye movement data collected during the symmetry tasks,
536 combined for all participants. The heatmaps are obtained from distributions of all valid eye
537 movement responses excluding blinks, collected within a 24 by 24 degree space covering the
538 stimulus. For visualisation, this space is split into 50 by 50 bins over which the two
539 dimensional histograms are computed. The display shows the normalised density values on an
540 8-bit intensity colour scale from blue to red shown inset, normalised to the percentage of
541 samples at the strongest red pixels with the maximum density. The heatmaps collected under
542 the free exploration condition presentation appear in the top panel and the active exploration
543 in the bottom panel. **A.** In the control distribution, gaze is centred around fixation. **B.** The
544 horizontal axis condition shows gaze also centred around fixation and extending along the H-
545 axis. **C.** The vertical axis condition shows gaze extended along the V-axis. **D.** 5 Ellipses
546 drawn within a zoomed in 12° stimulus area, corresponding to elliptical fits of the gaze
547 distributions. They correspond to the three free exploration cases: control (blue line),
548 horizontal (purple) and vertical symmetry axis (green), and two active exploration cases for
549 comparison, horizontal (purple dashed) and vertical symmetry axis (green dashed). Gaze is
550 seen to be elongated along the axis of symmetry where present, more so for the active cases.
551 The bottom panel contains the four active stimulus cases. **E.** For the right oblique symmetry
552 axis, gaze extends along this axis. **F.** The active horizontal axis gaze distribution is similar to
553 the free exploration in B. **G.** The vertical active condition is also similar to that for the free

554 exploration task in C. **H.** The left oblique axis condition shows gaze extending along the
555 corresponding axis.

556

557 **Figure 3:** Saccade properties for all participants during the free exploration task. **A.** Saccade
558 amplitude density, plotted following separation into 50-linearly spaced bins between 0-12° of
559 visual angle. Three conditions are shown, H (purple), V (green) and Control (dark blue) for all
560 plots. For all conditions, at least 85% of saccades are smaller than 4°, with half smaller than
561 1°. These proportions are similar for the three conditions. **B.** Saccade rates over the course of
562 a trial, in fifty 16.67ms intervals. Traces overlap for the three conditions and fall gradually
563 after an initial suppression around 250ms, and a peak around 500ms. **C.** Saccade direction
564 density for the group of participants. Samples are separated into 50 direction bins. There are
565 strong biases in the density distribution for the symmetric stimuli (H-purple and V-green).
566 Smaller biases along the cardinal axes can also be seen in the control condition (blue). **D.**
567 Group saccade density traces showing the mean and standard errors of the individual
568 continuous function fits based on data from the seven participants. The resulting traces
569 separate at the symmetry axes for the horizontal (purple) and vertical (green) cases when
570 compared to the control (dark blue) condition. The significance testing indicated by asterisks
571 at these axes takes the form of a two sample t-test at each direction bin between the control
572 and respective symmetrical condition. Axes of symmetry are indicated at the top of the figure
573 by black arrows in circles.

574

575 **Figure 4:** Saccade direction distributions for seven individual participants under the free
576 exploration task. Three conditions are plotted, horizontal (magenta traces) and vertical (green)
577 symmetry and the control asymmetric (blue). Each plot corresponds to one participant (S1-
578 S7). Notice that S1* and S2* are authors and therefore not naïve to the hypothesis. The total
579 number of saccades is also indicated for each subject. Overall, the individual data is consistent
580 with group fits in Figure 3, showing peaks along symmetry axes when present. Trends are
581 generally clearer when participants make a larger number of saccades.

582

583 **Figure 5:** Saccade patterns recorded during the symmetry discrimination task. Traces shown
584 combine data from six participants. **A.** The density of saccade amplitudes in 50 bins between
585 0-12° for the four symmetry axis conditions, Right Oblique (RO, dark blue), Vertical (V,
586 green), Left Oblique (LO, yellow) and Horizontal (H, purple). Traces show little difference

587 between conditions. Most saccades are small and the distributions peak between 0-0.5°. **B.**
588 Saccade rates over the course the 3s trials calculated in 16.67ms intervals show overlapping
589 traces for all four symmetry axis conditions. The trace colours are the same as in A. The peak
590 of the saccade rates occurs around 0.5s. The vertical dotted lines indicate the average reaction
591 times in the discrimination task for each of the conditions. **C.** Reaction times (right hand side
592 y-axis in grey) and percentage correct (left hand side y-axis) are plotted for the four axis
593 conditions. **D.** Saccade direction density plotted for the range of directions in 50 bins. In these
594 plots, direction peaks are seen to correspond exactly with the stimulus axes of symmetry. **E.**
595 Group saccade density traces showing the mean and standard errors of the individual
596 continuous function fits based on data from six participants. The black arrows with shown
597 within circles indicate the orientation of the four stimulus axes of symmetry in the
598 discrimination task. The resulting traces allow us to contrast orthogonal axes traces i.e.
599 horizontal (purple) against the vertical (green) cases and the right-oblique (dark blue) against
600 the left-oblique (yellow). The significance testing indicated at each of the axes (vertical
601 dashed lines) takes the form of a two-sample t-test across each direction bin in the distribution
602 between each of the orthogonal pairs of traces (H-V and RO-LO).

603

604 **Figure 6:** Saccade direction distributions for six individual participants under the active
605 exploration discrimination task. Four conditions are plotted together, horizontal (magenta
606 traces) and vertical (green), left oblique (orange) and right oblique (blue) symmetry. Again,
607 among the six participants (S1-S7), the first two, S1* and S2*, were non-naïve authors of the
608 present study. The total number of saccades is indicated for each participant. Notice that
609 subjects S4 and S7 made fewer saccades and therefore the distributions are less systematically
610 aligned with the axis of symmetry. On the contrary, these peaks are more prominent in
611 participants with a larger number of saccades. Overall, the individual data is consistent with
612 Figure 5 showing peaks along symmetry axes during the discrimination tasks.

613

614 **Figure 7:** Dynamic saccade selectivity calculated as the ratio of saccades recorded in a small
615 40° wedge centred on the direction of the axis of symmetry as a fraction of the total number
616 of saccades. The data is combined across all six participants. Selectivity is calculated within
617 12 bins of 250ms, and the statistical test for significance indicated by the asterisks is a non-
618 parametric Kruskal-Wallis test with a significance level of $P < 0.05$. The average reaction times
619 for each axis condition are plotted as black vertical dotted lines with the standard deviation

620 given by the grey shading. **A.** For the V axis of symmetry, the selectivity index is plotted
621 against time in milliseconds for the control (black line, diamonds), which shows lower
622 selectivity than both the free exploration (blue line, circles) and the active traces (red line,
623 squares). The traces are significantly different for both cases from around the bin centred on
624 875ms, with a consistent difference of about 0.2 in selectivity. **B.** For the horizontal axis of
625 symmetry, dynamic selectivity is plotted with traces in the same format as above. Baseline
626 selectivity in this axis orientation is higher even for the control due to H-biases and the active
627 and free exploration traces which are about 0.2 selectivity units above the control are only
628 significant in the bins centred on 1125 and 1625 ms respectively. **C.** Selectivity in the RO
629 direction for the active task (red trace, squares) is significantly higher than the control (black
630 trace, diamonds) from 625ms after onset. **D.** For the LO direction, the active task selectivity
631 (red trace, squares) is again significantly higher than the control (black trace, diamonds) from
632 625ms after onset.
633

634

635 **References**

636 **Apthorp D, and Bell J.** Symmetry is less than meets the eye. *CurrBiol* 25: R267-R268, 2015.

637 **Barlow HB, and Reeves BC.** The versatility and absolute efficiency of detecting mirror

638 symmetry in random dot displays. *Vision Res* 19: 783-793, 1979.

639 **Bertamini M, and Makin ADJ.** Brain Activity in Response to Visual Symmetry. *Symmetry-*

640 *Basel* 6: 975-996, 2014.

641 **Brainard DH.** The psychophysics toolbox. *Spat Vision* 10: 433-436, 1997.

642 **Carmody DP, Nodine CF, and Locher PJ.** Global Detection of Symmetry. *Perc& MotSkills*

643 45: 1267-1273, 1977.

644 **Delius JD, and Nowak B.** Visual Symmetry Recognition by Pigeons. *Psychological*

645 *Research-Psychologische Forschung* 44: 199-212, 1982.

646 **Driver J, Baylis GC, and Rafal RD.** Preserved figure-ground segregation and symmetry

647 perception in visual neglect. *Nature* 360: 73-75, 1992.

648 **Engbert R.** Microsaccades: a microcosm for research on oculomotor control, attention, and

649 visual perception. *Visual Perception, Part 1, Fundamentals of Vision: Low and Mid-Level*

650 *Processes in Perception* 154: 177-192, 2006.

651 **Engbert R, and Kliegl R.** Microsaccades uncover the orientation of covert attention. *Vision*

652 *Res* 43: 1035-1045, 2003.

653 **Findlay JM.** Global visual processing for saccadic eye movements. *Vision Res* 22: 1033-

654 1045, 1982.

655 **Giurfa M, Eichmann B, and Menzel R.** Symmetry perception in an insect. *Nature* 382: 458-

656 461, 1996.

657 **Hafed ZM, and Clark JJ.** Microsaccades as an overt measure of covert attention shifts.

658 *Vision Res* 42: 2533-2545, 2002.

659 **Hafed ZM, Goffart L, and Krauzlis RJ.** A Neural Mechanism for Microsaccade Generation

660 in the Primate Superior Colliculus. *Science* 323: 940-943, 2009.

661 **He PY, and Kowler E.** The role of location probability in the programming of saccades:

662 implications for "center-of-gravity" tendencies. *Vision Res* 29: 1165-1181, 1989.

663 **Hicheur H, Zozor S, Campagne A, and Chauvin A.** Microsaccades are modulated by both

664 attentional demands of a visual discrimination task and background noise. *JVis* 13: 2013.

665 **Itti L, and Koch C.** Computational modelling of visual attention. *Nature Reviews*

666 *Neuroscience* 2: 194-203, 2001.

- 667 **Itti L, Koch C, and Niebur E.** A model of saliency-based visual attention for rapid scene
668 analysis. *IEEE Trans Pattern Analysis Machine Intell* 20: 1254-1259, 1998.
- 669 **Jenkinson M, and Brady M.** A saliency-based hierarchy for local symmetries. *Image Vision*
670 *Comput* 20: 85-101, 2002.
- 671 **Kootstra G, de Boer B, and Schomaker LRB.** Predicting Eye Fixations on Complex Visual
672 Stimuli Using Local Symmetry. *Cognitive Computation* 3: 223-240, 2011.
- 673 **Kovesi P.** Symmetry and Asymmetry From Local Phase. In: *AI'97, Tenth Australian Joint*
674 *Conference on Artificial Intelligence* 1997, p. 185-190.
- 675 **Kowler E.** Eye movements: The past 25 years. *Vision Res* 51: 1457-1483, 2011.
- 676 **Laubrock J, Kliegl R, Rolfs M, and Engbert R.** When do microsaccades follow spatial
677 attention? *Attention Perception and Psychophysics* 72: 683-694, 2010.
- 678 **Locher PJ, and Nodine CF.** Influence of stimulus symmetry on visual scanning patterns.
679 *Perc Psychophys* 13: 408-412, 1973.
- 680 **Machilsen B, Pauwels M, and Wagemans J.** The role of vertical mirror symmetry in visual
681 shape detection. *JVis* 9: 11 11-11, 2009.
- 682 **Makin AD, Rampone G, Pecchinenda A, and Bertamini M.** Electrophysiological
683 responses to visuospatial regularity. *Psychophysiol* 50: 1045-1055, 2013.
- 684 **Marola G.** Using Symmetry for Detecting and Locating Objects in a Picture. *Computer*
685 *Vision Graphics and Image Processing* 46: 179-195, 1989.
- 686 **Martinez-Conde S, Macknik SL, Troncoso XG, and Dyar TA.** Microsaccades counteract
687 visual fading during fixation. *Neuron* 49: 297-305, 2006.
- 688 **Martinez-Conde S, Otero-Millan J, and Macknik SL.** The impact of microsaccades on
689 vision: towards a unified theory of saccadic function. *Nature Reviews Neuroscience* 14: 83-
690 96, 2013.
- 691 **McCamy MB, Otero-Millan J, Di Stasi LL, Macknik SL, and Martinez-Conde S.** Highly
692 Informative Natural Scene Regions Increase Microsaccade Production during Visual
693 Scanning. *Journal of Neuroscience* 34: 2956-2966, 2014.
- 694 **Norcia AM, Candy TR, Pettet MW, Vildavski VY, and Tyler CW.** Temporal dynamics of
695 the human response to symmetry. *J Vis* 2: 132-139, 2002.
- 696 **Osorio D.** Symmetry detection by categorization of spatial phase, a model. *Proceedings of the*
697 *Royal Society of London B* 263: 105-110, 1996.

- 698 **Otero-Millan J, Troncoso XG, Macknik SL, Serrano-Pedraza I, and Martinez-Conde S.**
699 Saccades and microsaccades during visual fixation, exploration, and search: Foundations for a
700 common saccadic generator. *JVis* 8: 2008.
- 701 **Pelli DG.** The VideoToolbox software for visual psychophysics: Transforming numbers into
702 movies. *Spat Vision* 10: 437-442, 1997.
- 703 **Poletti M, Listorti C, and Rucci M.** Microscopic Eye Movements Compensate for
704 Nonhomogeneous Vision within the Fovea. *CurrBiol* 23: 1691-1695, 2013.
- 705 **Rhodes G.** The evolutionary psychology of facial beauty. *Annu Rev Psychol* 57: 199-226,
706 2006.
- 707 **Rolfs M.** Microsaccades: Small steps on a long way. *Vision Res* 49: 2415-2441, 2009.
- 708 **Rucci M, Iovin R, Poletti M, and Santini F.** Miniature eye movements enhance fine spatial
709 detail. *Nature* 447: 851-854, 2007.
- 710 **Rucci M, McGraw PV, and Krauzlis RJ.** Fixational eye movements and perception. *Vision*
711 *Res* 118: 1-4, 2016.
- 712 **Rucci M, and Victor JD.** The unsteady eye: an information-processing stage, not a bug.
713 *Trends Neurosci* 38: 195-206, 2015.
- 714 **Spotorno S, Masson GS, and Montagnini A.** Fixational saccades during grating detection
715 and discrimination. *Vision Res* 2015.
- 716 **Treder MS.** Behind the Looking-Glass: A Review on Human Symmetry Perception.
717 *Symmetry-Basel* 2: 1510-1543, 2010.
- 718 **Treder MS, and Meulenbroek RGJ.** Integration of structure-from-motion and symmetry
719 during surface perception. *JVis* 10: 2010.
- 720 **Troncoso XG, McCamy MB, Jazi AN, Cui J, Otero-Millan J, Macknik SL, Costela FM,**
721 **and Martinez-Conde S.** V1 neurons respond differently to object motion versus motion from
722 eye movements. *Nature Communications* 6: 2015.
- 723 **Wagemans J.** Detection of Visual Symmetries. *Spat Vision* 9: 9-32, 1995.
- 724 **Wagemans J, Van Gool L, and d'Ydewalle G.** Detection of symmetry in tachistoscopically
725 presented dot patterns: effects of multiple axes and skewing. *Perc Psychophys* 50: 413-427,
726 1991.
- 727 **Wallach H, and O'Connell DN.** The kinetic depth effect. *J Exp Psychol* 45: 205-217, 1953.
- 728 **Wright D, Makin AD, and Bertamini M.** Right-lateralized alpha desynchronization during
729 regularity discrimination: hemispheric specialization or directed spatial attention?
730 *Psychophysiol* 52: 638-647, 2015.

- 731 **Yarbus AL.** *Eye Movements and Vision*. New York: Plenum Press, 1967.
- 732 **Yuval-Greenberg S, Merriam EP, and Heeger DJ.** Spontaneous Microsaccades Reflect
733 Shifts in Covert Attention. *Journal of Neuroscience* 34: 13693-13700, 2014.
- 734 **Zozor S, Amblard PO, and Duchene C.** Does eye tremor provide the hyperacuity
735 phenomenon? *Journal of Statistical Mechanics-Theory and Experiment* 2009.
- 736
- 737
- 738

739

APPENDIX

740 **1. Elliptical Gaussian fitting**

741 The Elliptical Gaussian Function was used to characterise the 300x300 pixel position density
 742 maps obtained by binning valid eye samples to obtain 2-dimensional distributions over a
 743 24x24 degree stimulus area. The function is defined by six principle parameters, and can be
 744 written in the form of the equation (1),

$$745 \quad f(x, y) = Amp \times \exp\left(-\frac{(x-x_0)^2}{2a^2} - \frac{theta \times (x-x_0)(y-y_0)}{ab} - \frac{(y-y_0)^2}{2b^2}\right), \quad (1)$$

746

747 A non linear least squares fitting procedure is applied to Equation (1) with group data
 748 collected under a given symmetry condition, implemented in Mathworks Matlab using the
 749 standard 'fit' function.

750

751 *Purpose:* For the 7 different experimental symmetry conditions described in the methods, the
 752 optimal 2D-Elliptical Gaussian parameters (*Amp*, x_0 and y_0 centre positions, a and b widths
 753 ie. the semi major and minor axes, and a *theta* parameter for orientation angle) are obtained. A
 754 validation of each fit is then carried out using an implementation of the method described in
 755 section 3 below. Five of these six parameters, excluding *Amp* were then used to generate
 756 ellipses enclosing approximately 68% of data points based on the position heat maps and
 757 assuming approximately Gaussian distributions (e.g. Figure 2D). The resulting distributions
 758 can be compared for the different test conditions. The results of the fits obtained for the seven
 759 experimental conditions, restricted to the width parameters, the corresponding coverage area
 760 (πab), and x and y centre positions, are shown in Table 1 below:

761

<i>Stimulus</i>	<i>x-width(a)</i>	<i>y-width(b)</i>	<i>Area</i> (deg^2)	<i>x-centre</i>	<i>y-centre</i>
Con (F)	2.03±1.63	2.98±0.1	19.0	-0.31	-0.12
V (F)	1.75±1.41	4.12±2.82	22.7	-0.33	-0.11
H (F)	5.25±0.13	1.75±0.02	28.9	-0.49	-0.04
RO (A)	3.19±0.18	2.94±0.15	29.4	-0.23	-0.35
V (A)	1.81±0.02	5.51±0.3	31.4	-0.54	-0.18
LO (A)	5.47±0.78	1.70±0.06	29.3	-0.01	0.02
H (A)	3.18±0.84	3.44±0.84	34.3	-0.33	0.13

762

763 **Table 1:** Semi major and minor axis-length and width parameters, the resulting coverage area of the
 764 ellipse, and the x - and y - centre positions for the ellipses fitted for the 7 task conditions. The first three
 765 containing (F) correspond to the free exploration cases, while the last four (A) correspond to the active

766 discrimination task. Widths in **bold** indicate cases where one axis was found to be wider than the other
767 when standard errors of the fits are taken into account. All fits return centre positions close to the
768 stimulus centre ($x_0 < 0.54^\circ$; $y_0 < 0.35^\circ$)

769

770 **2. Four peak Lorentzian function fitting**

771 The Lorentzian function is a continuous distribution characterised by three parameters per
772 peak. In our case, the use of four peaks allows a good fit to be made of all the data and uses
773 thirteen parameters. It was chosen here to model the one dimensional saccade direction
774 distributions measured in the experiments as it generates sharp peaks similar to those which
775 were observed in the data (see Figures 3C, 4, 5D and 6). There were no underlying
776 assumptions about the physiology with this function choice. Four peaks were chosen as the
777 minimal parametric complexity that could model the expected two dominant peaks
778 (corresponding to one axis of orientation of symmetry resulting in paired peaks in opposite
779 directions) in the possible presence of other smaller peaks. The identification of such
780 dominant peaks was required to compare the relative peak directions under our alternative
781 hypotheses on axes alignment that we sought to test. The function takes the form,

$$782 \quad f(\theta) = C + \sum_i \frac{Amp_i \times Sig_i^2}{Sig_i^2 + (\theta - \mu_i)^2}, i \in \{1, 2, 3, 4\} \quad (2)$$

783

784 C is a constant capturing the isotropically distributed background number of saccades. Amp_i
785 are the magnitudes of the four respective maxima in the distribution corresponding to four
786 different identified peaks. The direction at which each of the peaks is identified is given by μ_i .
787 Finally distribution width parameters for each peak Sig_i are used in the fitting bringing the
788 total number of fitted parameters to 13. The non linear fitting procedure is implemented in
789 Matlab, using the standard function ‘nlinfit’.

790

791 *Purpose:* The best fitting Amp , Sig and μ parameters corresponding to the cardinal directions
792 are compared to the control for the free exploration task, and orthogonal axes pairs are
793 compared in the active discrimination task. A two sample t-test at a significance level of
794 $P=0.05$ enables a direct comparison of the hypotheses that either: (a) peaks in directions of
795 saccades are not affected by the axis of symmetry, (b) peaks in directions preferentially occur
796 perpendicular to the axis of symmetry or (c) peaks in directions preferentially occur parallel to
797 the axis of symmetry. The fitted functions were tested and found to provide a satisfactory fit

798 for all the distributions when checked with the Kolmogorov-Smirnov test described in Section
799 3.

800

801 **3. Non-linear fitting validation**

802 A two sample Kolmogorov-Smirnov goodness of fit test was used to confirm that the
803 distribution functions used provided an acceptable fit of the experimental eye movement data
804 as described in sections 1-2 above. The test is a non parametric method to quantify the
805 difference between the cumulative distribution function of the reference (e.g. the Elliptical
806 Gaussian function or the multi-peak Lorentzian) and the measured distribution. This
807 difference generates the KS statistic and a corresponding probability distribution. The null
808 hypothesis is that the samples are drawn from the same distribution, and this is the test applied
809 for fits in this work, with the threshold set at a significance level of $P=0.05$. The test is
810 implemented in Mathworks Matlab.

811

812

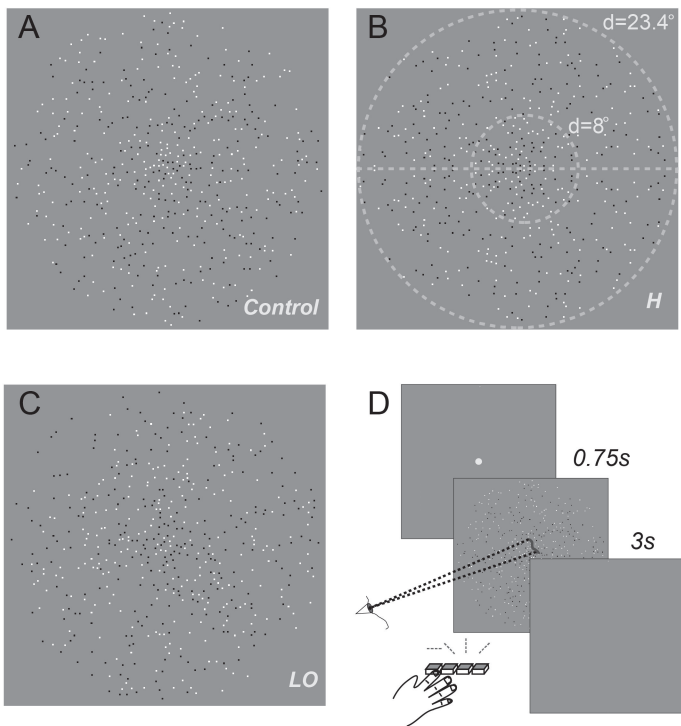


FIGURE 1
(one colum, 9cm)

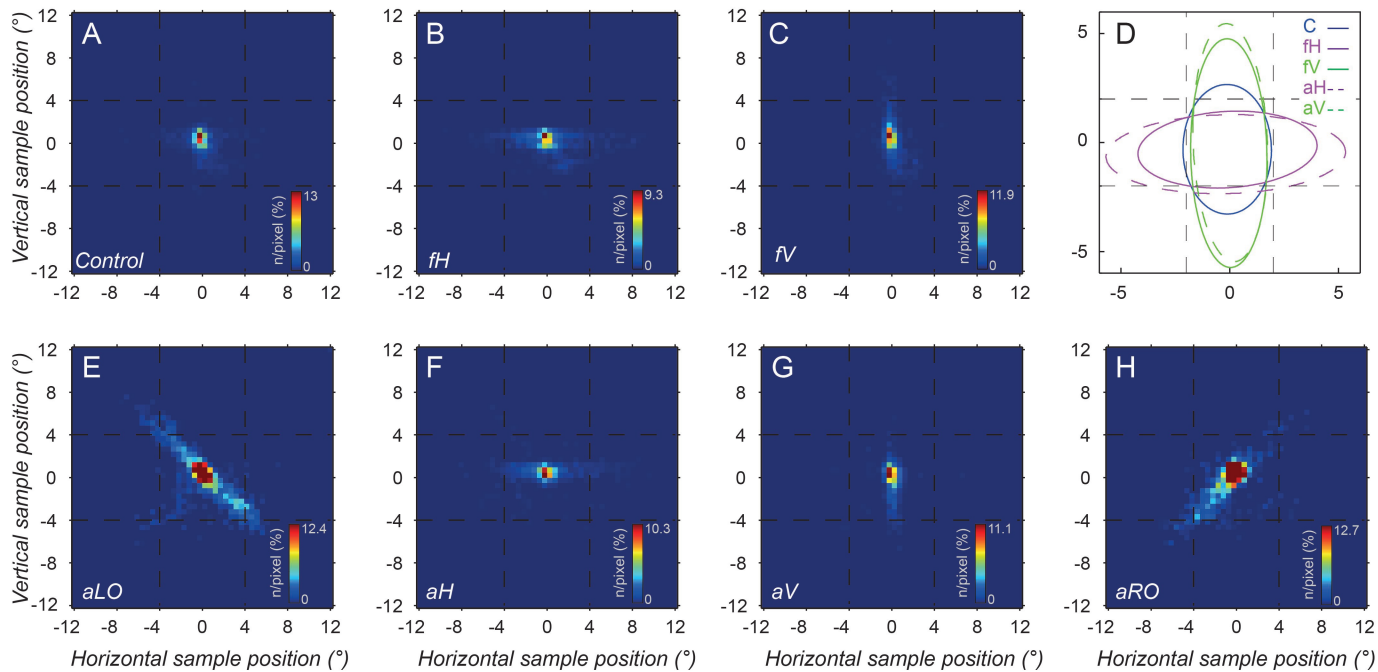


FIGURE 2
(2 columns, full length, 18cm)

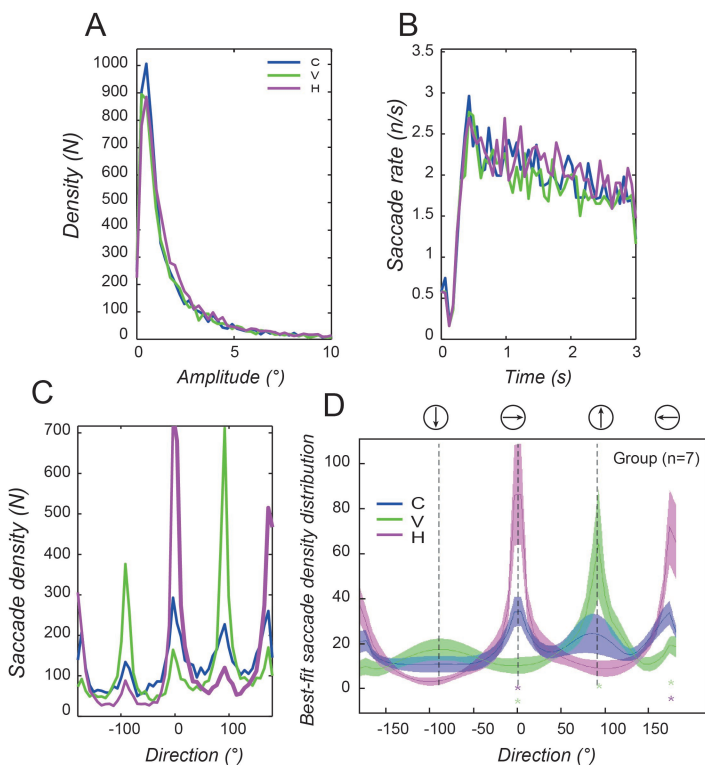


FIGURE 3
(single column 9cm)

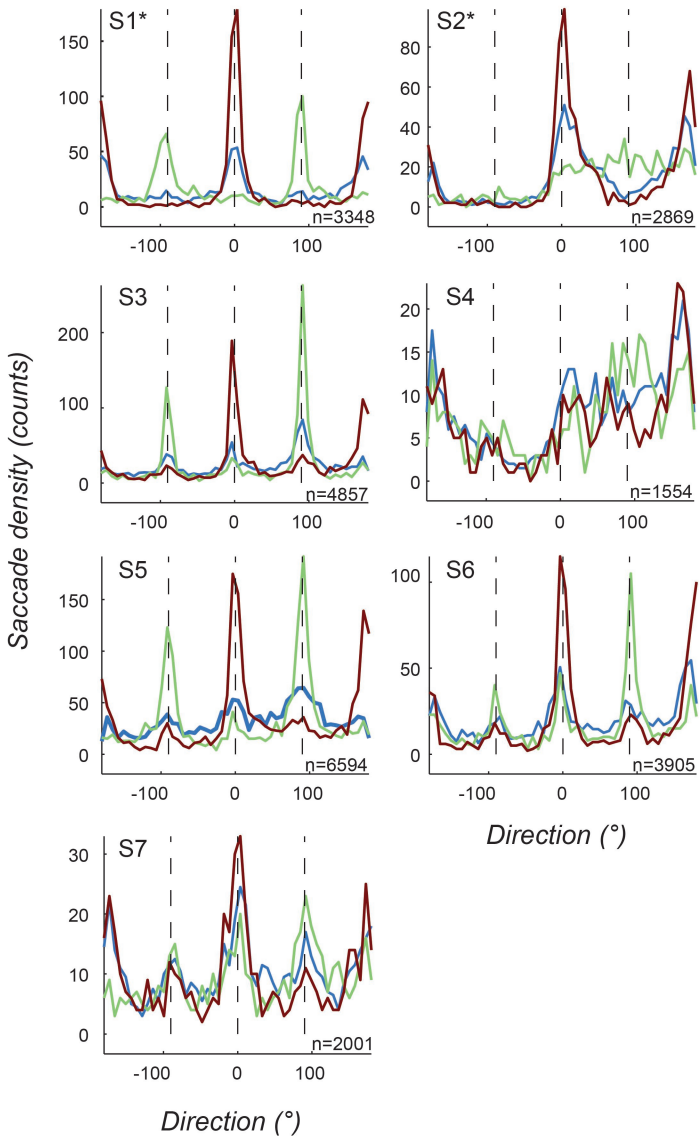


FIGURE 4
 (single column, 9cm)

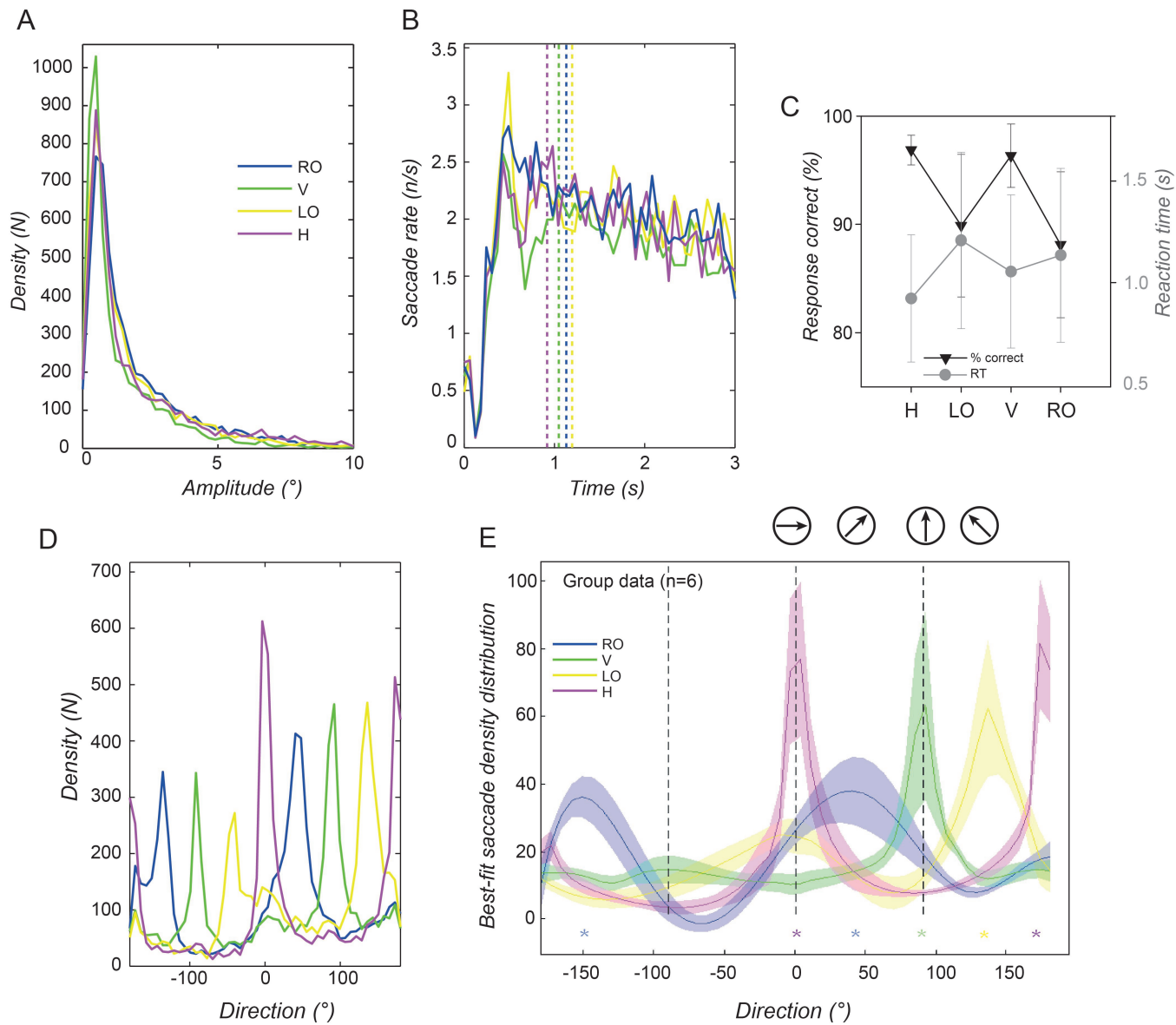


FIGURE 5
(2 columns full width 18cm)

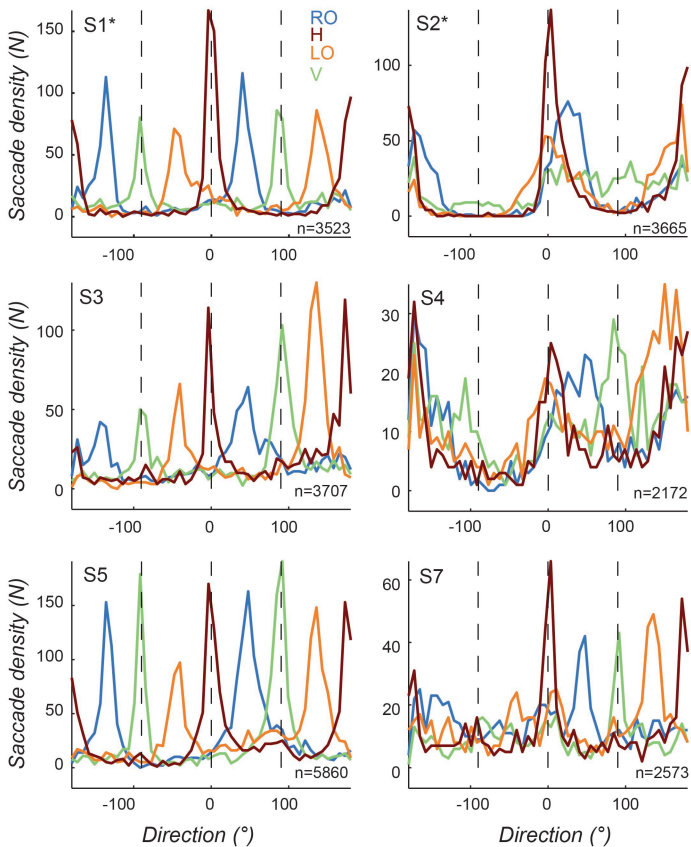


FIGURE 6
(single colum, 9cm)

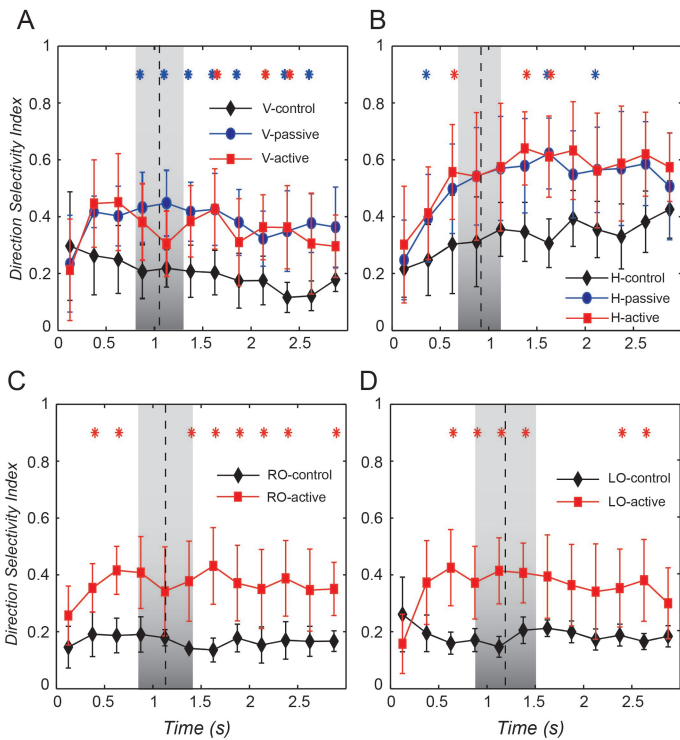


FIGURE 7
 (single column, 9cm)